Comparative analysis of hole transport in compressively strained InSb and Ge quantum well heterostructures

Ashish Agrawal, Michael Barth, Himanshu Madan, Yi-Jing Lee, You-Ru Lin, Cheng-Hsien Wu, Chih-Hsin Ko, Clement H. Wann, Dmitri Loubychev, Amy Liu, Joel Fastenau, Jeff Lindemuth, and Suman Datta

Citation: Applied Physics Letters **105**, 052102 (2014); doi: 10.1063/1.4892403
View online: http://dx.doi.org/10.1063/1.4892403
View Table of Contents: http://scitation.aip.org/content/aip/journal/apl/105/5?ver=pdfcov
Published by the AIP Publishing

Comparative analysis of hole transport in compressively strained InSb and Ge quantum well heterostructures

Ashish Agrawal,[1] Michael Barth,[1] Himanshu Madan,[1] Yi-Jing Lee,[2] You-Ru Lin,[2] Cheng-Hsien Wu,[2] Chih-Hsin Ko,[2] Clement H. Wann,[2] Dmitri Loubychev,[3] Amy Liu,[3] Joel Fastenau,[3] Jeff Lindemuth,[4] and Suman Datta[1]
[1]*Department of Electrical Engineering, The Pennsylvania State University, University Park, Pennsylvania 16802, USA*
[2]*Taiwan Semiconductor Manufacturing Company, Hsinchu 30078, Taiwan*
[3]*IQE, Inc., Bethlehem, Pennsylvania 18015, USA*
[4]*Lake Shore Cryotronics, Westerville, Ohio 43082, USA*

(Received 19 March 2014; accepted 16 July 2014; published online 5 August 2014)

Compressively strained InSb (s-InSb) and Ge (s-Ge) quantum well heterostructures are experimentally studied, with emphasis on understanding and comparing hole transport in these two-dimensional confined heterostructures. Magnetotransport measurements and bandstructure calculations indicate 2.5× lower effective mass for s-InSb compared to s-Ge quantum well at 1.9×10^{12} cm^{-2}. Advantage of strain-induced m* reduction is negated by higher phonon scattering, degrading hole transport at room temperature in s-InSb quantum well compared to s-Ge heterostructure. Consequently, effective injection velocity is superior in s-Ge compared to s-InSb. These results suggest s-Ge quantum well heterostructure is more favorable and promising p-channel candidate compared to s-InSb for future technology node. © *2014 AIP Publishing LLC*. [http://dx.doi.org/10.1063/1.4892403]

In recent times, there has been great interest in exploring the alternative to the Si channel in ultra-scaled transistors with alternate materials featuring lower transport mass and higher mobility. High performance III-V n-channel quantum well (QW) field effect transistors have been demonstrated with $In_{0.53}Ga_{0.47}As$ channel.[1] However, for complementary logic implementation, there is a significant challenge for identifying high mobility p-channel metal-oxide-semiconductor transistors (pMOS) candidates. Among the most attractive candidates for pMOS are compressively strained InSb, InGaSb, and Ge QW heterostructures, which feature high hole mobility.[2–4] The important parameters for designing the QW to enhance hole mobility are the percentage of strain in the channel, the valence band offset (VBO) between the QW and the barrier determining efficiency of carrier confinement, the effective mass and density of the carriers (Ns) in the light hole (*lh*) and heavy hole (*hh*) bands, and the lifting of the degeneracy between the *hh* and *lh* bands. Additionally, it is important to identify the dominant scattering mechanism, which limits the hole mobility of this two-dimensional hole gas (2DHG). It is imperative to understand, comprehensively, the transport in the QW, extract the dominant degradation mechanisms as a function of temperature and carrier density and subsequently suggest the key design parameters that would enable the selection of the best channel material.

In this paper, we systematically analyze and compare hole transport in 2% compressively strained InSb grown using molecular beam epitaxy (MBE) and 1.3% strained Ge quantum well heterostructure grown using rapid thermal chemical vapor deposition (RTCVD) (Fig. 1(a)). We performed six-band *k.p* bandstructure calculations to examine the effect of strain and quantization on the *hh* and *lh* subbands and the hole effective mass. Shubnikov-de Haas (SdH) magnetotransport measurements were performed as a function of magnetic field (0–9 T) at low temperature (T = 4 K) for the InSb QW, and in-plane hole effective mass was quantified using the oscillations observed in the 2DHG. Finally, using Hall measurements the hole carrier density and mobility were measured as a function of temperature for both the heterostructures (Fig. 1(b)). We use a transport lifetime model, based on relaxation time approximation, to examine the contributions of individual scattering mechanisms on the hole transport in the quantum well.[5] Although the QW

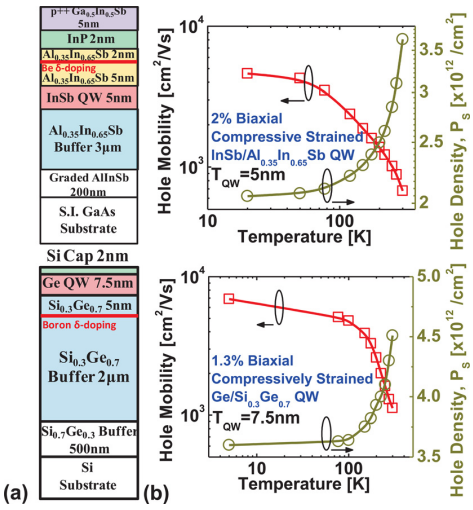

FIG. 1. (a) Schematic of the 2% compressively strained InSb QW heterostructure along with experimental Hall mobility and sheet density vs. temperature. (b) Schematic of 1.3% strained Ge QW heterostructure and experimental Hall mobility and hole density vs. temperature.

thickness for the two heterostructure systems is not identical, systematic extraction of effective mass and dominant scattering mechanisms give valuable insight into the fundamental material dependent transport properties.

A self-consistent Poisson-Schrodinger solver was used to calculate the valence subband structure of *hh* and *lh* bands in s-InSb and s-Ge QW heterostructure. Fig. 2(a) shows the energy band diagram of s-InSb and s-Ge QW heterostructure used in this work. Through the combined effect of strain and quantization in the QW, the *hh* and *lh* bands split. VBO between AlInSb barrier layer and strained InSb QW was ~0.25 eV providing efficient hole confinement. For the case of s-Ge QW, the Si cap provides a significantly higher VBO of 0.6 eV, ensuring more efficient confinement in Ge QW and supporting higher sheet carrier density without carrier spillout.

Due to the complex non-parabolic structure of the valence band, and to study the dependence of band warping and effective mass as a function of energy, it is important to investigate the E-*k* of individual subband in the plane of transport. Fig. 2(b) shows the isoenergy surface for the first *hh* subband in the s-InSb and s-Ge QW. Under biaxial stress, the energy surface is an ellipsoid with the energy contours in the x-y plane being circles, indicating that the band is isotropic in the plane of conduction for lower energy. At higher energy, the band becomes more anisotropic and the nonparabolicity increases with increasing energy. The effect of changing E-*k* and hence, the effective mass as a function of energy in the valence band has been accounted while solving Poisson-Schrodinger self-consistently and calculating the charge in the QW.

The in-plane hole effective mass was extracted using SdH magnetotransport measurements on the InSb QW heterostructure at low temperature (T = 4 K) and high magnetic fields, B (0–9 T). An oscillatory behavior can clearly be seen, superimposed on a parabolic dependence with magnetic field indicating high quality, defect free epitaxial growth of s-InSb QW. The oscillatory behavior is plotted vs. magnetic field in Fig. 3(a) correcting for the parabolic dependence, which occurs due to hole-hole interaction.[6] Oscillations were periodic with 1/B, a fast Fourier transform (FFT) (Fig. 3(a), inset) on the data shows that the oscillations

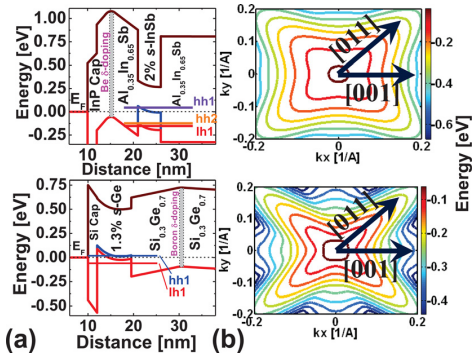

FIG. 2. (a) Six band *k.p* simulated energy band diagram of s-InSb and s-Ge QW heterostructure using self-consistent Poisson-Schrodinger solver. (b) 2D energy contour for first *hh* subband along the transport plane in s-InSb and s-Ge QW obtained using k.p calculations.

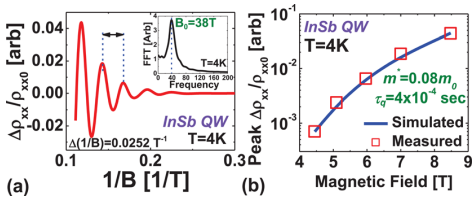

FIG. 3. (a) Measured sheet resistance of the InSb quantum well heterostructure as a function of magnetic field from 0–9 T, (b) Shubnikov-de Haas oscillations in sheet resistance as a function of 1/B at low temperature T = 4 K, inset shows FFT of the oscillations showing single frequency, indicating that only one *hh* subband is occupied at this sheet charge, (c) modeled and experimental peak $\Delta\rho_{xx}/\rho_{xx0}$ as a function of magnetic field used to extract the effective mass and quantum lifetime for the InSb QW heterostructure.

are harmonic with a single frequency implying the occupancy of the lowest energy hole subband. The frequency of the oscillations in the resistance as a function of the inverse magnetic field is related to the hole concentration as $N_S = 2q/\hbar\Delta(1/B) = 1.9 \times 10^{12}\,\mathrm{cm}^{-2}$.

Fig. 3(b) plots the experimental and modeled peak $\Delta\rho_{xx}/\rho_{xx0}$ as function of magnetic field. The extracted effective mass from the analysis is $0.08\,m_0$ at a sheet carrier density of $1.9 \times 10^{12}\,\mathrm{cm}^{-2}$ (from the period of SdH oscillations) and the extracted quantum lifetime, τ_q was 0.04 ps. The ratio of the transport lifetime from mobility (~0.22 ps) and the quantum lifetime is ~5.6. This low ratio indicates that the dominant scattering mechanism in the s-InSb QW heterostructure at low temperatures is isotropic, short range, and interface roughness (IR) scattering.

To compare the experimentally extracted m* for s-InSb with other QW heterostructures, the effective hole mass was compared with those derived from the band structure calculated using the six band *k.p* approach as discussed earlier (Fig. 4). The calculations were also extended to 1.3% strained Ge[7] and 1.8% strained InGaSb[3] QW heterostructure systems to benchmark and compare as a function of hole density. Experimentally measured effective mass has been overlayed on the modeled results for the respective material systems showing excellent agreement. 2.5× lower in-plane

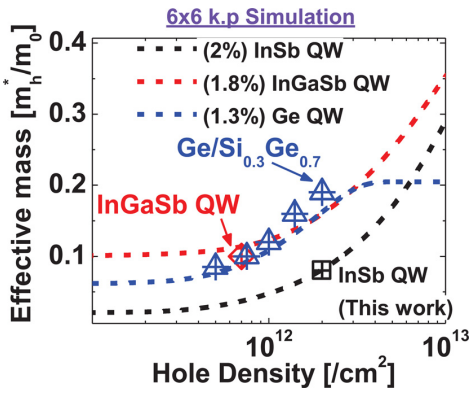

FIG. 4. In-plane hole effective mass as a function of hole sheet density simulated by 6-band *k.p* bandstructure solver for strained InSb QW, strained Ge and strained InGaSb QW heterostructure systems. Experimental data for strained Ge,[7] strained InGaSb,[3] and strained InSb(this work) has been overlayed to compare and benchmark.

effective mass was obtained with strained InSb QW compared to s-Ge and s-InGaSb for same hole density of $1.9 \times 10^{12}\,cm^{-2}$. It can be seen that the hole effective mass increases with increasing hole density, as a result of band nonparabolicity and warping. s-InSb QW has lowest effective mass for low hole density ($<5 \times 10^{12}/cm^2$) compared to strained Ge and InGaSb. At high hole density ($>5 \times 10^{12}/cm^2$), m* for s-Ge is 1.5× lower compared to s-InSb QW.

Fig. 5 shows the experimental and modeled hole sheet density extracted from Hall measurements of s-InSb and s-Ge QW sample as a function of temperature. The low-temperature carrier concentration in conjunction with a self-consistent Schrodinger-Poisson solver for the QW structure allows us to capture the temperature dependence of the measured carrier concentration, using the Boltzmann approximation model.[5] Excellent agreement is obtained between the experimental and modeled sheet carrier concentration as a function of temperature, allowing us to quantify the respective contributions from individual subbands. At low temperature, only the first *hh* subband contributes to the total hole concentration, whereas at room temperature, 10% of the total concentration was contributed by the second *hh* subband, along with a similar contribution from the buffer layer.

The primary scattering mechanisms in III-V heterostructures are well recognized and studied. The principal contributions to phonon scattering are from the polar optical phonons (POP) in the optical branch and the acoustic deformation potential (ADP) scattering. Specific to modulation doped quantum well heterostructures are the remote ionized impurity (RII) scattering from ionized dopants in the δ-doped layer and the interface roughness (IR) scattering. Both the intra- and inter-subband scattering rates were accounted due to the substantial contribution of the second subband at room temperature. The scattering rates for these processes were derived using Fermi's golden rule and combined using Mattheissen's rule.[5,8]

Fig. 6(a) shows a comparison of the combined scattering model with the temperature-dependent hole mobility of s-InSb and s-Ge QW heterostructures along with contributions from individual scattering mechanisms. At room temperature, the hole mobility shows significant temperature dependence, the transport being limited by POP scattering and ADP scattering. At low temperatures, temperature-independent IR scattering from the barrier-QW interface limits the hole mobility. The low energy phonons for InSb in addition to effect of strong quantization in thin QW significantly increases the overall phonon scattering rate, but the strain-induced effective mass reduction helps compensate the loss in mobility by reducing the transport effective mass and the DOS where holes could scatter into, resulting in enhanced hole transport in the QW. Fig. 6(b) shows the pareto plot depicting % contributions from various scattering mechanisms at room temperature.

The scattering analysis provides important insight into the fundamental transport characteristics of s-InSb and s-Ge QW heterostructures. Magnetotransport experiments have revealed 2.5× reduced m* for s-InSb compared to s-Ge QW heterostructure. In-spite of smaller hole transport mass, the experimental hole mobility for s-InSb is 55% lower compared to s-Ge QW. This is a result of higher polar optical phonon scattering and acoustic deformation potential scattering in InSb compared to Ge. The polar optical phonon energy in InSb is 25 meV,[5] 32% lower compared to Ge having optical phonon energy of 37 meV.[9] Additionally, the acoustic deformation potential, which indicates the strength of coupling between holes and lattice vibration, is 30 eV[10] for InSb, which is 100% higher compared to Ge featuring 15 eV.[11] These fundamental material parameters indicate that room temperature dominant phonon scattering is higher in InSb compared to Ge. Hence, it can be inferred that, for similar values of strain in InSb and Ge QW, the hole transport and mobility are likely to be superior for the s-Ge QW compared to s-InSb.

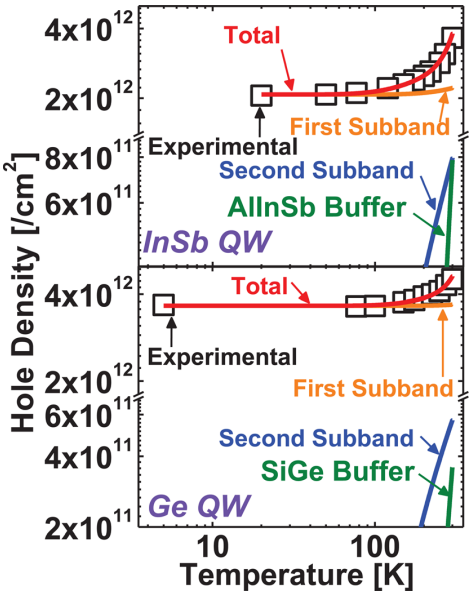

FIG. 5. (a) Experimental and modeled hole sheet density as a function of temperature for s-InSb and s-Ge QW heterostructure showing contributions from first and second *lh* subband and buffer layer conduction at room temperature.

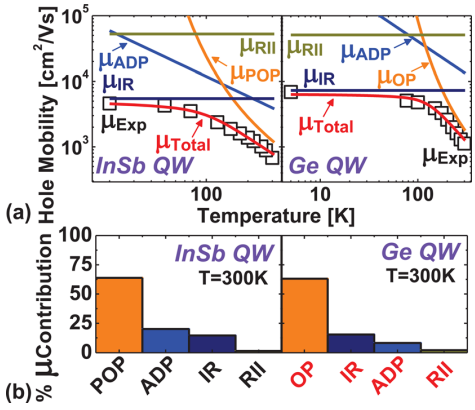

FIG. 6. (a) Experimental and modeled hole mobility as a function of temperature along with various scattering mechanisms. (b) Pareto plot of contribution from different scattering mechanisms to total mobility at 300 K for s-InSb and s-Ge QW heterostructures.

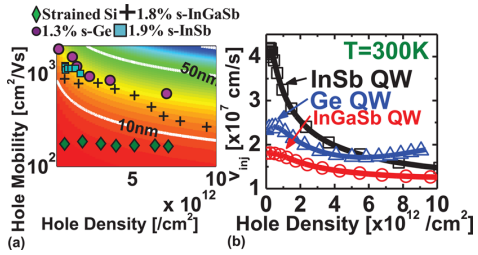

FIG. 7. (a) Mobility vs. hole density at room temperature overlayed on a contour map of ballistic mean free path for Strained Si,[4] s-InSb,[2] s-Ge,[4] and s-InGaSb[3] showing 5× higher hole mobility compared to s-Si. (b) Calculated effective injection velocity as a function of sheet charge density for s-InSb, s-Ge, and s-InGaSb QW heterostructure systems at 300 K.

Scaled FETs in the future may operate very close to the ballistic limit. Hence, the ballistic mean free path and the velocity at the source end, called as effective injection velocity (v_{inj}) will have to be enhanced. The 300 K mobilities vs. hole density overlayed on contour map of ballistic mean free path for s-Si,[4] s-InSb,[2] s-Ge,[4] and s-InGaSb[3] QW heterostructures is shown in Fig. 7(a). The ballistic mean free path is directly proportional to the mobility and the square root of the carrier concentration.[5] Hence, the QW heterostructures featuring high hole mobility have 3× larger hole mean free path than s-Si. In Fig. 7(b), the calculated v_{inj} as a function of sheet density for s-InSb, s-Ge and s-InGaSb QW heterostructures is shown. The v_{inj} depends on thermal velocity of holes that is inversely proportional to m* in addition to the degeneracy of the Fermi level in the valence band.[12–14] The significant increase in m* due to band nonparabolicity results in decreasing v_{inj} as a function of Ns for s-InSb and s-InGaSb QW systems. However, v_{inj} for s-Ge reduces for Ns of $5 \times 10^{12}/cm^2$, then increases at high Ns due to constant m* as extracted from k.p calculations and increasing degeneracy of Fermi level. Hence, in the absence of hole scattering, the lower effective mass enables s-InSb QW system as favorable for low Ns ($<5 \times 10^{12}/cm^2$). However, at high Ns ($>5 \times 10^{12}/cm^2$), s-Ge with higher v_{inj} shows promise as p-channel ballistic transistor.

We have examined the hole mobility and carrier concentration of 2% compressively strained InSb and 1.3% s-Ge quantum well heterostructure and over a range of temperature from 20 K to 300 K. Magnetotransport measurements were performed on the InSb QW and in-plane hole effective mass of 0.08 m_0 was extracted at T = 4 K and hole concentration of $1.9 \times 10^{12}\,cm^{-2}$, which is 60% lower than the experimental effective mass for compressively strained Ge QW and InGaSb QW at same sheet density. At high Ns, s-Ge features 1.5× lower transport mass compared to s-InSb QW. Hole density modeling as a function of temperature indicated major contribution from the first heavy hole subband, in addition to 1/10 contribution from parallel conduction in buffer layer at room temperature. Mobility-limiting scattering mechanisms were identified to be polar optical phonon scattering at room temperature and interface roughness scattering at low temperature. Advantage of strain-induced m* reduction was negated by 32% lower phonon energy and 100% higher acoustic deformation potential in s-InSb compared to s-Ge. In the ballistic limit, s-Ge QW outperforms other heterosystems with high v_{inj} at high Ns which stems from higher Fermi level degeneracy and constant m*. These results indicate s-Ge as favorable channel material for high performance p-channel MOSFETs for scaled technology nodes.

[1]M. Radosavljevic, G. Dewey, J. Fastenau, J. Kavalieros, R. Kotlyar, B. Chu-Kung, W. Liu, D. Lubyshev, M. Metz, K. Millard *et al.*, IEEE Int. Electron Devices Meet. **2010**, 6.1.1–6.1.4.
[2]M. Radosavljevic, T. Ashley, A. Andreev, S. Coomber, G. Dewey, M. Emeny, M. Fearn, D. Hayes, K. Hilton, M. Hudait *et al.*, IEEE Int. Electron Devices Meet. **2008**, 1–4.
[3]A. Nainani, B. Bennett, J. Brad Boos, M. Ancona, and K. Saraswat, J. Appl. Phys. **111**, 103706 (2012).
[4]R. Pillarisetty, B. Chu-Kung, S. Corcoran, G. Dewey, J. Kavalieros, H. Kennel, R. Kotlyar, V. Le, D. Lionberger, M. Metz *et al.*, IEEE Int. Electron Devices Meet. **2010**, 6–7.
[5]J. Orr, A. Gilbertson, M. Fearn, O. Croad, C. Storey, L. Buckle, M. Emeny, P. Buckle, and T. Ashley, Phys. Rev. B **77**, 165334 (2008).
[6]A. Houghton, J. Senna, and S. Ying, Phys. Rev. B **25**, 2196 (1982).
[7]K. Sawano, K. Toyama, R. Masutomi, T. Okamoto, N. Usami, K. Arimoto, K. Nakagawa, and Y. Shiraki, Appl. Phys. Lett. **95**, 122109 (2009).
[8]B. Ridley, J. Phys. C: Solid State Phys. **15**, 5899 (1982).
[9]R. A. Soref and G. Sun, Appl. Phys. Lett. **79**, 3639 (2001).
[10]I. Tsidilkovskii and K. Demchuk, Phys. Status Solidi (B) **44**, 293 (1971).
[11]T. Low, M.-F. Li, C. Shen, Y.-C. Yeo, Y. Hou, C. Zhu, A. Chin, and D. Kwong, Appl. Phys. Lett. **85**, 2402 (2004).
[12]M. Ferrier, R. Clerc, L. Lucci, Q. Rafhay, G. Pananakakis, G. Ghibaudo, F. Boeuf, and T. Skotnicki, IEEE Trans. Nanotechnol. **6**, 613 (2007).
[13]S. Datta, T. Ashley, J. Brask, L. Buckle, M. Doczy, M. Emeny, D. Hayes, K. Hilton, R. Jefferies, T. Martin *et al.*, IEEE Int. Electron Devices Meet. **2005**, 763–766.
[14]T. Ando, A. Fowler, and F. Stern, Rev. Mod. Phys. **54**, 437 (1982).